

A Pyrazolate-Supported $\text{Fe}_3(\mu_3\text{-O})$ Core: Structural, Spectroscopic, Electrochemical, and Magnetic Study

Dalice Piñero,[†] Peter Baran,^{†,‡} Roman Boca,^{§,||} Radovan Herchel,^{*,||,⊥} Michael Klein,[#] Raphael G. Raptis,^{*,†} Franz Renz,[#] and Yiannis Sanakis^{*,&}

Department of Chemistry and the Institute of Functional Nanomaterials, University of Puerto Rico, San Juan, PR 00931-3346, Department of Inorganic Chemistry, Slovak University of Technology, SK-812 37 Bratislava, Slovakia, Department of Chemistry, University of SS. Cyril and Methodius, Trnava, SK-91701 Slovakia, Department of Inorganic Chemistry, Palacký University, Křížkovského 10, CZ-77147 Olomouc, Czech Republic, Institute of Inorganic and Analytical Chemistry, Johannes Gutenberg-University, D-55099 Mainz, Germany, and Institute of Materials Science, NCRS “Demokritos”, 15310 Aghia Paraskevi, Athens, Greece

Received January 27, 2007

A comparison is made between the structural, spectroscopic, electrochemical, and magnetic properties of pyrazolate versus carboxylate complexes $[\text{Fe}_3(\mu_3(\mu_3\text{O})(\mu\text{-LL})_6\text{Cl}_3)]^{2-}$ containing the $\text{Fe}_3(\mu_3\text{-O})$ -motif. While the $\text{Fe}_3(\mu_3\text{-O})$ -cores are structurally indistinguishable in the two types of complexes, their magnetic properties deviate from the expected values as a result of a through-pyrazole contribution to the overall antiferromagnetic exchange with $J_1/hc = -80.1 \text{ cm}^{-1}$ and $J_2/hc = -72.4 \text{ cm}^{-1}$, or $J_1/hc = 70.6 \text{ cm}^{-1}$ and $J_2/hc = -80.8 \text{ cm}^{-1}$, ($H_{\text{ex}} = -J_1(S_1S_2 + S_2S_3) - J_2S_1S_3$). The magnetic properties of the pyrazolate complexes are further tuned by an antisymmetric exchange interaction term.

Introduction

Carboxylates constitute one of the widest families of transition-metal complexes and have been associated with numerous studies in all aspects of coordination chemistry. Their ubiquitous presence in Nature makes them an essential ligand in bioinorganic chemistry and an obvious choice when a chelating or bridging ligand is required. Since some early investigations of metal–metal interactions and magnetic exchange,¹ carboxylate complexes have an uninterrupted history as well in what has now become known as materials chemistry. In recent years, elegant studies of electron transfer and ground-breaking work in the new field of single molecule

magnets have been carried out using transition metal carboxylates.^{2,3}

In the course of our investigations of transition-metal pyrazolate chemistry, we became aware of the existence of a structural parallel between carboxylate and pyrazolate complexes of the same nuclearity: quite similar Pd–Pd distances are found in the trinuclear $[\text{Pd}(\mu\text{-O}_2\text{CR})_2]_3$ and $[\text{Pd}(\mu\text{-pz})_2]_3$ complexes (pz = pyrazolato, $\text{C}_3\text{H}_3\text{N}_2^-$, or substituted pyrazolato anion).^{4,5} Additional examples exist in the

* To whom correspondence should be addressed. E-mail: raphael@adam.uprr.pr (R.G.R.), radovan.herchel@upol.cz (R.H.), sanakis@ims.demokritos.gr (Y.S.).

[†] University of Puerto Rico.

[‡] Present address: Department of Chemistry, Juniata College, Huntingdon, PA 16652.

[§] Slovak University of Technology.

^{||} Palacký University.

[⊥] University of SS. Cyril and Methodius.

[#] Johannes Gutenberg-University.

[&] NCRS “Demokritos”.

(1) (a) Figgis, B. N.; Robertson, G. B. *Nature* **1965**, *205*, 694. (b) Beckett, R.; Cotton, R.; Hoskins, B. F.; Martin, R. L.; Vince, D. G. *Aust. J. Chem.* **1969**, *22*, 2527.

(2) (a) Londergan, C. H.; Salsman, J. C.; Ronco, S.; Dolkas, L. M.; Kubiak, C. P. *J. Am. Chem. Soc.* **2002**, *124*, 6236. (b) Londergan, C. H.; Kubiak, C. P. *J. Phys. Chem. A* **2003**, *107*, 9301.

(3) (a) Christou, G.; Gatteschi, D.; Hendrickson, D. N.; Sessoli, R. *MRS Bull.* **2000**, 66 and references therein. (b) Soler, M.; Wernsdorfer, W.; Foltling, K.; Pink, M.; Christou, G. *J. Am. Chem. Soc.* **2004**, *126*, 2156. (c) Mishra, A.; Wernsdorfer, W.; Abboud, K. A.; Christou, G. *J. Am. Chem. Soc.* **2004**, *126*, 15648. (d) Milios, C. J.; Vinslava, A.; Whittaker, A. G.; Parsons, S.; Wernsdorfer, W.; Christou, G.; Perlepes, S. P.; Brechin, E. K. *Inorg. Chem.* **2006**, *45*, 5272.

(4) (a) Baran, P.; Marrero, C. M.; Pérez, S.; Raptis, R. G. *Chem. Commun.* **2002**, 1012. (b) Umakoshi, K.; Yamauchi, Y.; Nakamiya, K.; Kojima, T.; Yamasaki, M.; Kawano, H.; Onishi, M. *Inorg. Chem.* **2003**, *42*, 3907.

(5) (a) Smart, M. L.; Skapski, A. C. *J. Chem. Soc., Chem. Commun.* **1970**, 658. (b) Djalina, N. N.; Dargina, C. V.; Sobolev, A. N.; Buslaeva, T. M.; Romm, I. P. *Koord. Khim.* **1993**, *19*, 57. (c) Bancroft, D. P.; Cotton, F. A.; Falvello, L. R.; Shwotzer, W. *Polyhedron* **1988**, *7*, 615. (d) Cotton, F. A.; Han, S. *Rev. Chim. Miner.* **1985**, *22*, 277.

literature, as between the tetranuclear Cu^{I} carboxylates $[\text{Cu}(\mu\text{-O}_2\text{CPh})_4]$ and $[\text{Cu}(\mu\text{-O}_2\text{CCF}_3)_4]$ on one hand and the pyrazolate $[\text{Cu}(\mu\text{-3,5-Ph}_2\text{-pz})_4]$ on the other.^{6,7} Replacement of one ligand by another, while the metal-core motif remains mostly unperturbed, can have significant effects on the physical properties of the metal centers, as both their electronic structure and their electronic and magnetic communication are influenced by the donor–acceptor properties and orbital symmetry of the ligands. Perlepes et al. have shown that substitution of a hydroxide or cyanide by an azide bridge inverts the sign of magnetic exchange in nonanuclear Ni^{2+} , Co^{2+} , and Fe^{2+} clusters.⁸ Considering the central role of carboxylates as ligands in coordination and materials chemistry—particularly in the fast expanding field of single-molecule magnets³—the development of a parallel class of structurally related pyrazolates would open up a number of new possibilities. To investigate further this structural parallel and its accompanying effects, we turned our attention to one of the best known motifs in carboxylate chemistry, namely the $\text{M}_3(\mu_3\text{-O})$ core, which includes examples of most transition metals.⁹

A variety of $[\text{Fe}_3(\mu_3\text{-O})(\mu\text{-O}_2\text{CR})_6\text{L}_3]$ complexes have been studied with regard to the magnetic and electronic interactions of their three paramagnetic metal centers.¹⁰ The long metal–metal distances within the $\text{Fe}_3(\mu_3\text{-O})$ unit preclude direct metal–metal bonding, and the magnitude of the O-mediated antiferromagnetic exchange among them is determined by the Fe–O bond lengths.¹¹ Trinuclear $[\text{Fe}_3(\mu_3\text{-O})(\mu\text{-O}_2\text{CR})_6\text{L}_3]$ complexes have proven excellent starting

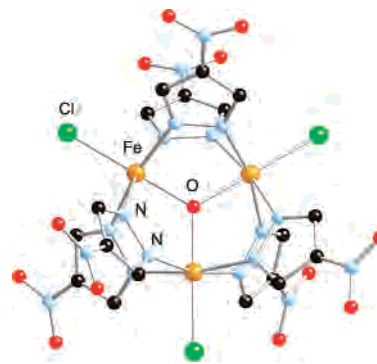


Figure 1. Ball-and-stick diagram of anions **1**.

materials for the synthesis of higher nuclearity clusters, taking advantage of the lability of carboxylate ligands.¹²

Here we report on the synthesis, characterization, X-ray crystal structure, and infrared and electrochemical study of the trinuclear anion $[\text{Fe}_3(\mu_3\text{-O})(\mu\text{-4-O}_2\text{N-pz})_6\text{Cl}_3]^{2-}$ (**1**) (Figure 1), as its Et_3NH^+ (**a**), Bu_4N^+ (**b**), or PPh_4^+ (**c**) salts, along with the electron paramagnetic resonance (EPR), the Mössbauer spectroscopy, magnetic susceptibility, and magnetization studies for **1a**. We present a comparison among the best studied $[\text{Fe}_3(\mu_3\text{-O})(\mu\text{-LL})_6\text{L}_3]$ complexes with LL = carboxylate on one hand and the analogous LL = pyrazolate complexes reported here on the other to better elucidate the relationship between the physical properties and the structural environment of the Fe_3O motif.

Experimental Section

Synthesis. Reagents were purchased from Sigma-Aldrich and used without further purification. The anhydrous Fe^{III} salts were stored in a glovebox compartment under argon. The ligand 4- $\text{O}_2\text{N-pzH}$ was synthesized according to a literature method.¹³ Infrared, ^1H NMR, and UV–vis spectra were recorded on a Nicolet FT-IR 6000, Bruker ADVANCE DRX-500, and Varian CARY 500 Scan, respectively.

$(\text{Et}_3\text{NH})_4[\text{Fe}_3(\mu_3\text{-O})(\mu\text{-4-NO}_2\text{-pz})_6\text{Cl}_3]\text{Cl}_2$, **1a.** A flask is charged with 0.750 g (4.62 mmol) of anhydrous FeCl_3 , 30 mL of CH_2Cl_2 , and 1.569 g (13.87 mmol) of 4- $\text{O}_2\text{N-pzH}$ under an argon atmosphere, forming a partially soluble yellow solid. Dropwise addition of NEt_3 (1.611 mL, 11.5 mmol) to the reaction mixture under air changes the solution color to dark red. X-ray-quality single crystals were obtained by slow Et_2O vapor diffusion into the CH_2Cl_2 solution; yield, 52%, mp = 192 °C. Anal. Found (calcd) for **1a**: C, 34.82 (34.98); H, 5.21 (5.31); N, 21.23 (21.37). UV/vis ($\text{CH}_2\text{-Cl}_2$): λ_{max} = 291 nm. IR (KBr disk, cm^{-1}): ν = 1489 (s), 1407 (s), 1279 (s), 1163 (s), 1035 (s), 1008 (s), 976 (m), 888 (m), 837 (w), 815 (s), 759 (s), 682 (w), 626 (s), 600 (s), 551 (m), 476 (s). ^1H NMR (CDCl_3): 30.87 ppm. The sample of **1a** used for magnetic susceptibility measurements was prepared from 99.99% FeCl_3 .

$(\text{Bu}_4\text{N})_2[\text{Fe}_3(\mu_3\text{-O})(\mu\text{-4-NO}_2\text{-pz})_6\text{Cl}_3]\cdot 0.5\text{MeOH}\cdot\text{H}_2\text{O}$, **1b.** Complex **1b** is prepared similarly to **1a** in thf solvent, using a 1 M $\text{Bu}_4\text{NOH/MeOH}$ solution instead of NEt_3 . X-ray-quality single crystals are obtained by slow Et_2O vapor diffusion into a CH_2Cl_2

- (6) (a) Drew, M. G. B.; Edwards, D. A.; Richards, R. *J. Chem. Soc., Dalton Trans.* **1977**, 299. (b) Cotton, F. A.; Dikarev, E. V.; Petrukina, M. A. *Inorg. Chem.* **2000**, *39*, 6072. (c) Reger, D. L.; Huff, M. F.; Wolfe, T. A.; Adams, R. D. *Organometallics* **1989**, *8*, 848. (d) Rodesiler, P. F.; Amma, E. L. *Chem. Commun.* **1974**, 599.
- (7) Ardizzoia, G. A.; Cenini, S.; LaMonica, G.; Masciocchi, N.; Maspero, A.; Moret, M. *Inorg. Chem.* **1998**, *37*, 4284.
- (8) (a) Papaefstathiou, G. S.; Escuer, A.; Vicente, R.; Font-Bardia, M.; Solans, X.; Perlepes, S. P. *Chem. Commun.* **2001**, 2414. (b) Papaefstathiou, G. S.; Perlepes, S. P.; Escuer, A.; Vicente, R.; Font-Bardia, M.; Solans, X. *Angew. Chem., Int. Ed.* **2001**, *40*, 884. (c) Boudalis, A. K.; Donnadieu, B.; Nastopoulos, V.; Clemente-Juan, J.-M.; Mari, A.; Sanakis, Y.; Tuchagues, J.-P.; Perlepes, S. P. *Angew. Chem., Int. Ed.* **2004**, *43*, 2266.
- (9) Cannon, R. D.; White, R. P. *Prog. Inorg. Chem.* **1988**, *36*, 195.
- (10) (a) Blake, A. B.; Fraser, L. R. *J. Chem. Soc., Dalton Trans.* **1975**, 193. (b) Degang, F.; Guoxiong, W.; Wenxia, T. *Polyhedron* **1993**, *12*, 2459. (c) Bond, A. M.; Clark, R. J. H.; Humphrey, D. G.; Panayiotopoulos, P.; Skelton, B. W.; White, A. H. *J. Chem. Soc., Dalton Trans.* **1998**, 1845. (d) Wu, R.; Pouraz, M.; Sowrey, F. E.; Anson, C. E.; Woadlo, S.; Powell, A. K.; Jayasooriya, U. A.; Cannon, R. D.; Nakamoto, T.; Katada, M.; Sano, H. *Inorg. Chem.* **1998**, *37*, 1913. (e) Sowrey, F. E.; Tilford, C.; Woadlo, S.; Anson, C. E.; Powell, A. K.; Bennington, S. M.; Montfrooij, W.; Jayasooriya, U. A.; Cannon, R. D. *J. Chem. Soc., Dalton Trans.* **2001**, 862. (f) Hibbs, P.; van Koningsbruggen, P. J.; Arif, A. M.; Shum, W. W.; Miller, J. S. *Inorg. Chem.* **2003**, *42*, 5645. (g) Sreerama, S. G.; Pal, S. *Eur. J. Inorg. Chem.* **2004**, 4718. (h) Raptoulou, C. P.; Sanakis, Y.; Boudalis, A. K.; Psycharis, V. *Polyhedron* **2005**, *24*, 711. (i) Johnson, M. K.; Powell, D. B.; Cannon, R. D. *Spectrochim. Acta* **1981**, *37A*, 995. (j) Montri, L.; Cannon, R. D. *Spectrochim. Acta* **1985**, *41A*, 643. (k) Dziobkowski, C. T.; Wroblewski, J. T.; Brown, D. B. *Inorg. Chem.* **1981**, *20*, 671. (l) Gavrilenko, K. S.; Addison, A.; Thompson, L.; Pavlishchuk, V. V. *Theor. Exp. Chem.* **2004**, *40*, 214. (m) Stadler, C.; Daub, J.; Köhler, J.; Saalfrank, R. W.; Coropceanu, V.; Schünemann, V.; Ober, C.; Trautwein, A. X.; Parker, S. F.; Poyraz, M.; Inomata, T.; Cannon, R. D. *J. Chem. Soc., Dalton Trans.* **2001**, 3373. (n) Boudalis, A. K.; Sanakis, Y.; Dahan, F.; Hendrich, M.; Tuchagues, J.-P. *Inorg. Chem.* **2006**, *45*, 443.
- (11) Gorun, S. M.; Lippard, S. J. *Inorg. Chem.* **1991**, *30*, 1625.

- (12) (a) Yao, H.; Wang, J.; Ma, Y.; Waldmann, O.; Du, W.; Song, Y.; Li, Y.; Zheng, L.; Decurtins, S.; Xin, X. *Chem. Commun.* **2006**, 1745. (b) Benelli, C.; Parsons, S.; Solan, G. A.; Winpenny, R. E. P. *Angew. Chem., Int. Ed. Engl.* **1996**, *35*, 1825. (c) Taft, M.; Wernsdorfer, W.; Følting, K.; Pink, M.; Christou, G. *J. Am. Chem. Soc.* **2004**, *126*, 2156. (13) Maresca, K. P.; Rose, D. J.; Zubieta, J. *Inorg. Chim. Acta* **1997**, *260*, 83.

Table 1. Crystallographic Data for **1a–c**

param	1a	1b	1c
empirical formula	C ₄₂ H ₇₆ Cl ₅ Fe ₃ N ₂₂ O ₁₃	C _{50.5} H ₈₈ Cl ₃ Fe ₃ N ₂₀ O _{14.5}	C ₆₆ H ₅₂ Cl ₃ Fe ₃ N ₁₈ O ₁₃ P ₂
fw	1442.05	1481.31	1641.10
temp (K)	298	299	298(2)
wavelength (Å)	0.710 73	0.710 73	0.710 73
cryst syst	orthorhombic	monoclinic	monoclinic
space group	<i>Pbcn</i>	<i>P2₁/c</i>	<i>P2₁/n</i>
<i>a</i> (Å)	24.344(4)	17.811(3)	17.532(3)
<i>b</i> (Å)	10.672(2)	15.399(2)	18.109(3)
<i>c</i> (Å)	25.978(4)	26.573(4)	24.150(4)
β (deg)	90	101.809(3)	106.755(3)
<i>V</i> (Å ³)	6748.7(2)	7134.0(2)	7342(2)
<i>Z</i>	4	4	4
<i>D</i> (calcd) (Mg m ⁻³)	1.419	1.379	1.485
abs coeff (mm ⁻¹)	0.904	0.785	0.811
cryst size (mm)	0.14 × 0.10 × 0.10	0.29 × 0.22 × 0.15	0.16 × 0.14 × 0.14
indpndt reflns/ <i>I</i> > 2σ(<i>I</i>)	4852/3055	15 937/9304	12 952/6696
<i>R</i> / <i>R</i> _w	0.0497/0.1183	0.0677/0.1451	0.0472/0.0846
<i>F</i> (000)	2996	3104	3348
GoF	1.003	1.044	0.902

Table 2. Selected Bond Lengths (Å) and Angles (deg) for **1a–c**

param	1a	1b	1c
Fe···Fe	3.267(1), 3.280(1)	3.269(4)–3.287(1)	3.265(1)–3.292(2)
Fe–O	1.885(4), 1.894(2)	1.889(3)–1.898(3)	1.878(2)–1.904(2)
Fe–N	2.129(3)–2.152(4)	2.116(3)–2.161(4)	2.116(4)–2.149(3)
Fe–X	2.280(2), 2.284(2)	2.272(1)–2.294(1)	2.263(1)–2.291(1)
Fe–O–Fe	120.4(1), 119.1(2)	120.6(1)–119.4(1)	119.7(1)–120.3(1)
O–Fe–X	177.7(1), 180.000(1)	177.63(9)–178.98(9)	177.51(8)–179.9(1)

solution of the dark red reaction product; yield >20%, mp = 245 °C. Anal. Found (calcd) for **1b**: C, 41.29 (40.94); H, 5.84 (5.99); N, 19.13 (18.92).

(Ph₄P)₂[Fe₃(μ₃-O)(μ-4-NO₂-pz)₆Cl₃], **1c**. A flask is charged with 0.189 g (0.35 mmol) of [Ph₄P][FeCl₄], 15 mL of CH₂Cl₂, and 0.132 g (1.17 mmol) of 4-O₂N-pzH. Dropwise addition of NEt₃ (0.162 mL, 1.16 mmol) turns the mixture to a dark red solution. X-ray-quality single crystals were obtained by slow Et₂O diffusion into the CH₂Cl₂ solution; yield >40%. mp = 277 °C. Anal. Found (calcd) for **1c**: C, 48.63 (49.02); H, 3.69 (3.64); N, 14.51 (14.70).

X-ray Crystallography. X-ray diffraction data, taken from a single crystal mounted atop a glass fiber, were collected on a Bruker AXS SMART 1K CCD area detector with graphite-monochromated Mo Kα radiation (λ = 0.710 73 Å) at room temperature using the program SMART-NT¹⁴ and processed by SAINT-NT.¹⁵ An empirical absorption correction was applied by the program SADABS. The structures were solved by direct method and refined by full-matrix least-squares methods on *F*².¹⁶ All non-hydrogen atoms were refined anisotropically, while H-atoms were placed in calculated positions with their thermal parameters riding on those of their C atoms. Crystallographic details for **1a–c** are summarized in Table 1.

Electrochemical experiments were performed with a BAS CV 50-W voltammetric analyzer, using a nonaqueous Ag/AgNO₃ reference electrode for which the ferrocene/ferricenium couple occurs at 0.200 V, Pt auxiliary electrode, and Pt working electrode. Magnetic functions were measured with a SQUID apparatus (Quantum Design) at *B* = 0.1 T from 2.0 to 300 K, and the isothermal magnetization was measured at *T* = 1.8 and 4.5 K, respectively. A correction to the underlying diamagnetism was estimated on the basis of Pascal constants as χ_{dia} = −9.91 × 10^{−9} m³ mol^{−1} for **1a**. X-band EPR measurements were performed with powdered samples or acetone solutions of **1a** with a Bruker ER

200D instrument equipped with an ESR-9 Oxford cryostat and an Anritsu microwave frequency counter. Mössbauer measurements were recorded on a constant-acceleration conventional spectrometer with a ⁵⁷Co (Rh matrix) source. Variable-temperature spectra were obtained by using Oxford cryostats, operating at 4.2–300 K. Isomer shift values (δ) are quoted relative to iron foil at 293 K.

Results and Discussion

The reactions of FeCl₃ (or PPh₄FeCl₄) with excess 4-O₂N-pzH and base (NEt₃, or Bu₄NOH) give the corresponding salts of **1**, which are recrystallized from CH₂Cl₂/Et₂O yielding analytically pure samples. An ~50% excess of pyrazole in the reaction mixture improves the crystalline product yield. The X-ray crystallographic analyses show that the all three dianions **1** contain six-coordinate Fe^{III} centers forming an Fe₃(μ₃-O) core, supported by six bridging pyrazolates and three terminal chlorides (Figure 1). Table 2 summarizes important bond lengths and angles for **1a–c**, respectively. While the molecular symmetry of anion **1** is *D*_{3h}, consistent with the presence of a single resonance for all 12 protons in the ¹H NMR/CDCl₃ spectrum, its crystallographic symmetry is 2-fold (**1a**) or lower (**1b,c**): Complex **1a** crystallizes on 2-fold axis running along an Fe–O bond, with one short (3.267(1) Å) and two long (3.280(1) Å) Fe···Fe distances. Whole trinuclear complex dianions are present in the asymmetric units of **1b,c**. The trinuclear complex dianion **1** packs efficiently with two PPh₄⁺ counterions in the crystal lattice, while the lattices of the Bu₄N⁺ salt **1b** include interstitial solvent molecules. When the smaller NEt₃H⁺ counterion is employed, the crystal lattice of **1a** includes two interstitial [NEt₃H]Cl, besides the Fe₃ dianion. Inspection of packing diagrams shows that the shortest intermolecular contact in **1a** is an O···O distance of 2.951 Å between two NO₂ groups, while the shortest intermolecular Fe···Fe

(14) SMART-NT, version 5.0; Bruker AXS: Madison, WI, 1998.

(15) SAINT-NT, version 5/6.0; Bruker AXS: Madison, WI, 1999.

(16) SHELXTL-NT, version 5.1; Bruker AXS: Madison, WI, 1998.

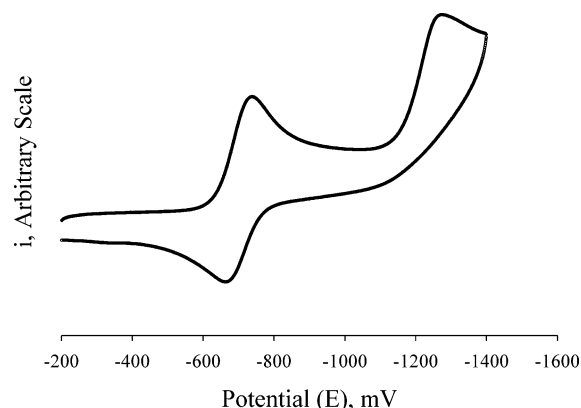
Table 3. Fe–O and Fe⋯Fe Distances for Selected $[\text{Fe}_3(\mu_3\text{-O})(\mu\text{-LL})_6\text{X}_3]$ Complexes

complex	Fe–O (Å)	Fe⋯Fe (Å)	ref
$[\text{Fe}_3\text{O}(\text{O}_2\text{CCH}_3)_6(\text{isoxazole})_3]\text{ClO}_4$	1.901, 1.894	3.286, 3.284	10f
$[\text{Fe}_3\text{O}(\text{O}_2\text{CPh})_6(\text{CH}_2\text{OH})_3]\text{NO}_3$	1.890, 1.907	3.274, 3.300, 3.284	10b
$[\text{Fe}_3\text{O}(\text{O}_2\text{CPh})_5(\text{salox})(\text{MeOH})_2]$	1.855, 1.882, 1.944	3.254, 3.251, 3.327	10h
$[\text{Fe}_3\text{O}(\text{O}_2\text{CPh})_6(\text{py})_3]\text{NO}_3$	1.9084	3.306	10c
$[\text{Fe}_3\text{O}(\text{bamen})_3]^+$	1.898, 1.911	3.299, 3.301	10g
$[\text{Fe}_3\text{O}(\text{piv})_6(\text{MeOH})_3]^+$	1.905	3.274	10a
$[\text{NaFe}_3\text{O}(\text{O}_2\text{CPh})_5(\text{pic})_2(\text{EtOH})_2(\text{H}_2\text{O})_2](\text{ClO}_4)_2$	1.897, 1.917, 1.933	3.283, 3.285, 3.371	10n

approach is of 7.995 Å. Similarly, the shortest intermolecular contacts, also between NO_2 groups, are $\text{O}\cdots\text{O}$ of 3.301 Å in **1b** and 2.949 Å in **1c**, while the shortest intermolecular $\text{Fe}\cdots\text{Fe}$ contacts for **1b,c** are 9.882 and 10.307 Å, respectively.

The Fe–O and $\text{Fe}\cdots\text{Fe}$ distances of **1** (Table 2) fall within the narrow ranges of the corresponding distances reported for analogous $\text{Fe}_3(\mu_3\text{-O})$ complexes of carboxylate or oxime ligands: 1.855–1.944 and 3.251–3.327 Å, respectively (Table 3).¹⁰ Similarly, the infrared $\nu_{\text{as}}(\text{Fe–O})$ bands for **1** occur at 626 cm^{-1} (598 cm^{-1} for $\nu_{\text{as}}(\text{Fe–}^{18}\text{O})$), also comparable to those reported for carboxylate analogues, 595–635 cm^{-1} (Table 4).^{10d,i,j}

Cyclic voltammetric analysis of **1b** (Figure 2) in the +1.000 to –1.440 V window shows one reversible reduction at $E_{1/2} = -0.703$ V (vs Fc^+/Fc), followed by an irreversible one at –1.246 V, which remains irreversible at 218 K. The voltammetric results are consistent with earlier studies of $\text{Fe}_3(\mu_3\text{-O})$ carboxylates showing a strongly ligand-dependent reversible reduction to the formally mixed-valent $\text{Fe}^{\text{III}}_2\text{Fe}^{\text{II}}$ species at $E_{1/2}$ values between –0.09 and –0.76 V.^{10c} The $E_{1/2}$ values of the pyrazolate complex $[\text{Fe}_3(\mu_3\text{-O})(\mu\text{-O}_2\text{N-pz})_6\text{Cl}_3]^{2-}$ (**1b**) are shifted negative compared to those of the isoivalent carboxylates $[\text{Fe}_3(\mu_3\text{-O})(\mu\text{-O}_2\text{CR})_6\text{L}_3]^+$. This is largely due to the charge difference between the dianionic **1** (with three terminal chlorides) and the monocationic carboxylate complexes (with three neutral terminal ligands, L).

**Figure 2.** Cyclic voltammogram (0.03 M $\text{Bu}_4\text{NPF}_6/\text{CH}_2\text{Cl}_2$, 295 K, Pt-working electrode, Ag/AgNO_3 reference, 100 mV/s sweep) of **1b** from –200 to –1400 mV, vs Fc/Fc^+ .

Mössbauer spectra from powdered samples of **1a** were recorded in the 4.2–300 K temperature range and zero external magnetic fields. Representative spectra are shown in Figure 3. At $T > 20$ –30 K, the spectra comprise one relative symmetric quadrupole doublet with $\delta = 0.43$ (1) mm s^{-1} and $\Delta E_{\text{Q}} = 1.02(2)$ mm s^{-1} at 78 K. No noticeable

Table 4. Infrared $\nu_{(\text{Fe–O})}$ Stretches for Selected $[\text{Fe}_3(\mu_3\text{-O})(\mu\text{-LL})_6\text{X}_3]$ Complexes

complex	$\nu_{\text{as}}(\text{Fe}_3\text{O})$	ref
1a	626 (^{18}O ; 598)	this work
$[\text{Fe}_3\text{O}(\text{O}_2\text{CH})_6(\text{H}_2\text{O})_3]\text{NO}_3$	595	10i
$[\text{Fe}_3\text{O}(\text{O}_2\text{CCH}_3)_6(\text{H}_2\text{O})_3]\text{ClO}_4$	609	10i
$[\text{Fe}_3\text{O}(\text{O}_2\text{CCH}_3)_6(\text{py})_3]\text{NO}_3$	604	10i
$[\text{Fe}_3\text{O}(\text{O}_2\text{CCH}_3)_6(\gamma\text{-pic})]\text{ClO}_4$	605	10i
$[\text{Fe}_3\text{O}(\text{O}_2\text{CCH}_3)_6(\text{py})_3][\text{FeCl}_4]$	600 (^{18}O ; 580)	10j
$[\text{Fe}_3\text{O}(\text{O}_2\text{CCH}_3)_6(\text{py})_3]\text{ClO}_4$	635	10d
$[\text{Fe}_3\text{O}(\text{O}_2\text{CPh})_6(\text{py})_3]\text{ClO}_4$	622	10e
$[\text{Fe}_3\text{O}(\text{O}_2\text{CCH}_3)_6(\text{H}_2\text{O})_3]\text{ClO}_4$	520	10k

dependence of ΔE_{Q} on temperature is observed. On the other hand, the isomer shift decreases as the temperature increases ($\delta = 0.32(1)$ mm s^{-1} , at 293 K). The temperature dependence of the isomer shift is attributed to the second-order Doppler effect.¹⁷ The value of isomer shift in the whole temperature range is consistent with high-spin ferric ions in N/O coordination environment. For temperatures below 20 K, an asymmetric line broadening is observed and is attributed to the onset of relaxation effects. Magnetic susceptibility studies (see below) indicate that the ground state of **1a** is characterized by $S = 1/2$, which is the only thermally occupied state at liquid-helium temperature. As the spin–lattice relaxation rate decreases at liquid-helium temperatures, nonzero effective magnetic fields are induced at the iron nuclei, thus affecting the spectra.¹⁸ Because the line broadening is larger for the lower energy line, a negative sign for the largest component of the electron field gradient (EFG) tensor is inferred.¹⁸ For complex **1a** the isomer shift fall at the lower end of the $\text{Fe}^{\text{III}}_3\text{O}$ -carboxylate range (Table 5), indicating an increased degree of covalency for the present compounds compared to typical carboxylates.¹⁰ On the other hand, the high quadrupole splitting value reflects the axial (locally C_{4v}) ClN_4O coordination environment of the Fe atoms of **1a**, compared to the pseudooctahedral O_6 coordination of the carboxylate complexes listed in Table 5.

The overall temperature dependence of the effective magnetic moment for **1a** (Figures 4 and 5) indicates a sizable antiferromagnetic exchange. However, the low-temperature data reach a μ_{eff} value of 1.3 μ_{B} , lower than the theoretical limit of 1.7 μ_{B} for an $S = 1/2$ molecular spin predicted by isotropic exchange. In addition, the magnetization curve deviates progressively from the theoretical prediction when only the isotropic exchange is taken into account. The analysis of the magnetic susceptibility data (both χ vs T and M vs H) as well as the EPR spectra (below) requires the presence of non-Heisenberg interactions. These could be (a)

(17) Greenwood, N. N.; Gibb, T. C. In *Mössbauer Spectroscopy*; Chapman and Hall Ltd.: London, 1971.(18) Blume, M. *Phys. Rev. Lett.* **1965**, *14*, 96.

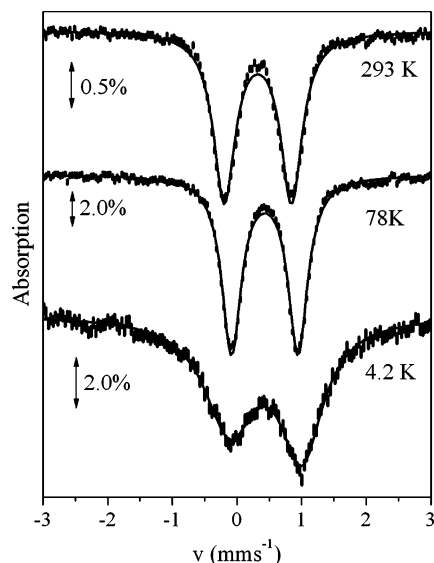


Figure 3. Mössbauer spectra of **1a** at 293, 78, and 4.2 K.

single ion anisotropy (zero field splitting D_i), (b) asymmetric (pseudodipolar) interaction D_{ij} , or (c) antisymmetric interaction (d_{ij}).^{19,20} With regard to the magnetic properties, the three terms induce the same effects, namely lowering of g_{eff} for the $S = 1/2$ ground state and axial EPR signals with extremely low g_{\perp} values. Consequently, the EPR results cannot be used as an argument for favoring one term over the other two. Rather, antisymmetric exchange (AE) is favored here on the basis of quantitative considerations on the basis of the different effects that the terms a–c have on the exchange coupling scheme of **1a**. Both D_i and D_{ij} mix states with higher S values into the ground $S = 1/2$ state, inducing the aforementioned phenomena (low g_{eff} and g_{\perp}). Therefore, to a first approximation, the effects of these terms on the magnetic properties depend on the ratios D_i/J and D_{ij}/J , respectively (J is the average value of the J_{ij} 's). The J_{ij} values can be accurately estimated from the fitting of the χ vs T data. However, to achieve a good fitting of the magnetic data, unreasonably large D_i or D_{ij} values had to be assumed (because the magnitude of J leads to relatively large energy separation between the ground $S = 1/2$ states and the $S > 1/2$ states). Antisymmetric exchange, on the other hand, mixes the two $S = 1/2$ ground states; the effects on the magnetic properties of **1a** depend approximately on the ratio d_{ij}/δ , where δ is a measure of the nonequivalence between the J_{ij} values (lowering of the D_{3h} symmetry). As a result, the effects of AE are more pronounced for more symmetric triangles, where δ is close to zero and even a small value of d_{ij} can induce large anisotropies. Apart from the point–dipolar interaction (which has the same effects

as the D_{ij} term), all the other terms arise from spin–orbit coupling, which is small (albeit nonzero) for $\text{Fe}^{3+}(S = 5/2)$ ions.

Therefore, a spin-Hamiltonian for an isosceles triangle with the isotropic, AE and molecular-field correction has been postulated:

$$\hat{H} = -J_1(\mathbf{S}_1 \cdot \mathbf{S}_2 + \mathbf{S}_2 \cdot \mathbf{S}_3) - J_2(\mathbf{S}_1 \cdot \mathbf{S}_3) + \mathbf{d}_{12} \cdot (\mathbf{S}_1 \times \mathbf{S}_2) + \mathbf{d}_{23} \cdot (\mathbf{S}_2 \times \mathbf{S}_3) + \mathbf{d}_{31} \cdot (\mathbf{S}_3 \times \mathbf{S}_1) + \mu_B B_a g (\hat{S}_{1a} + \hat{S}_{2a} + \hat{S}_{3a}) - zj \langle \hat{S}_a \rangle_T (\hat{S}_{1a} + \hat{S}_{2a} + \hat{S}_{3a}) \quad (1)$$

Here J_i are the isotropic exchange interaction parameters, \mathbf{d}_{ij} are corresponding antisymmetric vectors, zj is a common molecular-field parameter, and $\langle S_a \rangle_T$ is a thermal average of the spin projection in the a -direction. For the magnetic field vector in the polar coordinates defined as $\vec{\mathbf{B}}_a = B(\sin \theta \cos \varphi, \sin \theta \sin \varphi, \cos \theta)$ the molar magnetization was calculated as

$$M_{a,\text{mol}} = -N_A \frac{\sum_i (\sum_k \sum_l C_{ik}^+ (Z_a)_{kl} C_{li}) \exp(-\epsilon_{a,i}/kT)}{\sum_i \exp(-\epsilon_{a,i}/kT)} \quad (2)$$

where Z_a is the matrix element of the Zeeman term for the a -direction of the magnetic field and C values are the eigenvectors resulting from the diagonalization of the complete spin Hamiltonian matrix in local basis set of uncoupled kets (spin $S_i = 5/2$ for each center).

Since a powder sample was used, the averaged molar magnetization was calculated as an orientational average using the qromb subroutine:²¹

$$M_{\text{mol}} = 1/4\pi \int_0^{2\pi} \int_0^\pi M_{a,\text{mol}} \sin \theta \, d\theta \, d\varphi \quad (3)$$

Since the averaged spin in eq 1 needs eigenvectors, the equation has been solved by an iterative, time-demanding procedure. The data were fitted simultaneously for the temperature dependence and the field dependence of the magnetization with the assumptions that following hold: (a) The antisymmetric vector is equal for each pair, $\mathbf{d}_{12} = \mathbf{d}_{23} = \mathbf{d}_{31} = \mathbf{d}$, and only the z -component was assumed to be nonzero, $d_x = d_y = 0$. (b) The g factors for Fe^{III} are fixed at $g_x = g_y = g_z = 2.0$. This leaves four free parameters, namely J_1 , J_2 , d_z , and zj . Two different parameter sets were found for **1a**, which is a common feature.^{10n,22} First, for $J_1 > J_2$: $J_1/\text{hc} = -80.1 \text{ cm}^{-1}$; $J_2/\text{hc} = -72.4 \text{ cm}^{-1}$; $|d_z|/\text{hc} = 5.09 \text{ cm}^{-1}$; $zj/\text{hc} = -0.326 \text{ cm}^{-1}$ (Figure 4). Second, for $J_1 < J_2$: $J_1/\text{hc} = -70.6 \text{ cm}^{-1}$; $J_2/\text{hc} = -80.8 \text{ cm}^{-1}$; $|d_z|/\text{hc} = 9.87 \text{ cm}^{-1}$; $zj/\text{hc} = -0.325 \text{ cm}^{-1}$ (Figure 5). The average values for the isotropic exchange are in both cases quite similar, $J_{\text{av}}/\text{hc} = -77.5 \text{ cm}^{-1}$ and $J_{\text{av}}/\text{hc} = -74.0 \text{ cm}^{-1}$, respectively. The intermolecular interaction zj was found to be of antiferromagnetic nature and of the same value in both cases.

- (19) (a) Dzyaloshinski, I. *J. Phys. Chem. Solids* **1958**, *4*, 241. (b) Moriya, T. *Phys. Rev.* **1960**, *120*, 91. (c) Tsukerblat B. S.; Belinskii, M. I.; Fainzil'berg, V. E. *Sov. Sci. Rev. B: Chem.* **1987**, *9*, 337. (d) Bencini, A.; Gatteschi, D. *Mol. Phys.* **1982**, *47*, 161.
- (20) (a) Boca, R. *Coord. Chem. Rev.* **2004**, *284*, 757. (b) Boca, R. *Theoretical Foundations of Molecular Magnetism*; Elsevier: Amsterdam, 1999. (c) Bencini, A.; Gatteschi, D. *EPR of Exchanged Coupled Systems*; Springer-Verlag: Berlin, 1990.

(21) *Numerical recipes in Fortran*; <http://www.nr.com>.

(22) Jones, D. H.; Sams, J. R.; Thompson, R. C. *J. Chem. Phys.* **1984**, *81*, 440.

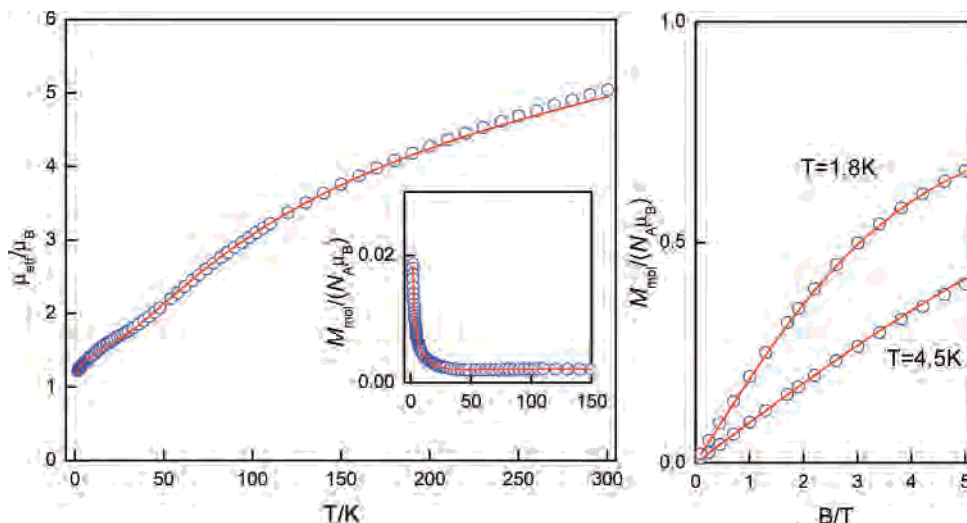


Figure 4. Temperature dependence of the effective magnetic moment (left, $B = 0.1$ T) and magnetization (right, $T = 1.8$ and 4.5 K) for **1a**. Inset: Temperature dependence of the molar magnetization. Key: open circles, experimental data; red solid line, best-fit for $J_1/hc = -80.1$ cm^{-1} , $J_2/hc = -72.4$ cm^{-1} , $|d_z|/hc = 5.09$ cm^{-1} , and $zj/hc = -0.326$ cm^{-1} .

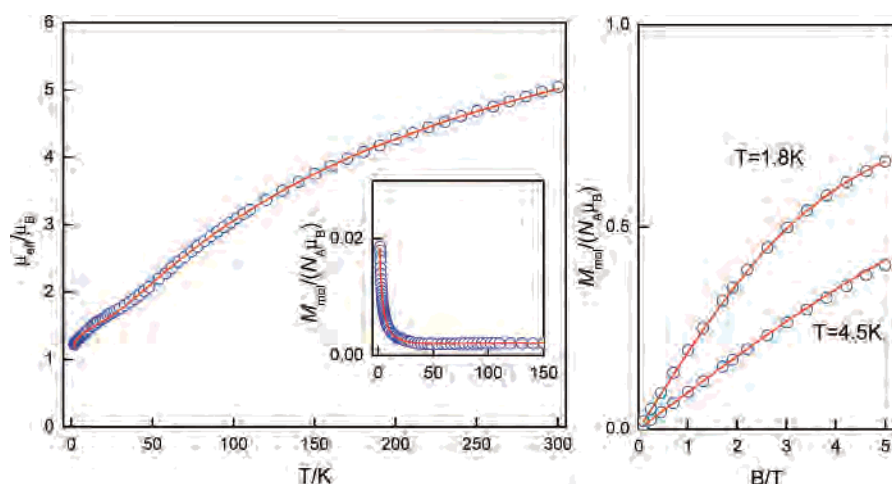


Figure 5. Temperature dependence of the effective magnetic moment (left, $B = 0.1$ T) and magnetization (right, $T = 1.8$ and 4.5 K) for **1a**: open circles, experimental data; solid line, best-fit for $J_1/hc = -70.6$ cm^{-1} , $J_2/hc = -80.8$ cm^{-1} , $|d_z|/hc = 9.87$ cm^{-1} , and $zj/hc = -0.325$ cm^{-1} .

Table 5. Mössbauer Isomer Shift (δ) and Quadrupole Splitting (ΔE_Q) Values for Selected $[\text{Fe}_3(\mu_3\text{-O})(\mu\text{-LL})_6\text{Cl}_3]$ Complexes

complex	δ , mm s^{-1}	ΔE_Q , mm s^{-1}	ref
1a	0.43(1)	1.02(2)	this work, $T = 78$ K
	0.32(1)	1.04(2)	this work, $T = 293$ K
$[\text{Fe}_3\text{O}(\text{O}_2\text{CCH}_3)_6(\text{H}_2\text{O})_3]\text{ClO}_4$	0.53	0.74	10k, $T = 21$ K
	0.42	0.58	10k, $T = 295$ K
$[\text{Fe}_3\text{O}(\text{O}_2\text{CCH}_2\text{CO}_2)_3(\text{H}_2\text{O})_3]\text{ClO}_4$	0.52	0.72	10k, $T = 21$ K
	0.41	0.58	10k, $T = 295$ K
$[\text{Fe}_3\text{O}(\text{O}_2\text{CCH}_2\text{CH}_2\text{CO}_2)_3(\text{H}_2\text{O})_3]\text{ClO}_4$	0.53	0.81	10k, $T = 22$ K
	0.42	0.67	10k, $T = 295$ K
$[\text{Fe}_3\text{O}(\text{O}_2\text{CCHCHCO}_2)_3(\text{H}_2\text{O})_3]\text{ClO}_4$	0.51	0.88	10k, $T = 20$ K
	0.42	0.79	10k, $T = 295$ K
$[\text{Fe}_3\text{O}(\text{o-phthalate})_3(\text{H}_2\text{O})_3](\text{o-phthalate})_{0.5}$	0.52	0.82	10k, $T = 22$ K
	0.41	0.81	10k, $T = 295$ K
$[\text{Fe}_3\text{O}(\text{m-phthalate})_3(\text{H}_2\text{O})_3](\text{m-phthalate})$	0.53	0.93	10k, $T = 22$ K
	0.42	0.79	10k, $T = 295$ K
$[\text{Fe}_3\text{O}(\text{dittetrazole})_3]\text{NO}_3$	0.44	1.10	10m, $T = 4.2$ K
$[\text{Fe}_3\text{O}(\text{O}_2\text{CPh})_6(\text{CH}_3\text{OH})_3]\text{NO}_3$	0.31	0.346	10b, $T = \text{room temp}$
$[\text{NaFe}_3\text{O}(\text{O}_2\text{CPh})_5(\text{pic})_2(\text{EtOH})_2(\text{H}_2\text{O})_2](\text{ClO}_4)_2$	0.51	0.70	10n, $T = 78$ K
	0.40	0.59	10n, $T = 298$ K

The plots of the lowest energy levels for both parameter sets (Figure S5, Supporting Information) reveal that the ground state is $S = 1/2$ with effective g factors $g_{\parallel,\text{eff}} = 2.0$ and $g_{\perp,\text{eff}} = 0.84$ (for both fits). Such a low value for $g_{\perp,\text{eff}}$ is the result of the antisymmetric exchange.

The analyses of magnetic data for several analogous to **1** carboxylate complexes containing the $\text{Fe}_3(\mu_3\text{-O})$ motif have yielded J values in the range of -34.3 to -64.4 cm^{-1} , while a complex of a polydentate- N_5 ligand gave $J/hc = -82.0$ cm^{-1} (Table 6).^{10b,f-h,l,n}

Table 6. Magnetic Exchange Coupling Constants^a for Selected [Fe₃(μ₃-O)(μ-LL)₆X₃] Complexes

complex	<i>J</i> /hc, cm ⁻¹	ref
1a	-80.1, -72.4, -70.6, -80.8	this work
[Fe ₃ O(O ₂ CCH ₃) ₆ (isoxazole) ₃]ClO ₄	-58.8, -34.3	10f
[Fe ₃ O(O ₂ CPh) ₆ (CH ₃ OH) ₃]NO ₃	-54.12	10b
[Fe ₃ O(O ₂ CPh) ₅ (salox)(MeOH) ₂]	-54.6	10h
[Fe ₃ O(bamen) ₃] ⁺	-82.0	10g
[Fe ₃ O(O ₂ CCH ₃) ₆ (pyz) ₃]ClO ₄	-64.6	10l
[Fe ₃ O(O ₂ CCH ₃) ₆ (H ₂ O) ₃]NO ₃	-54	10i
[NaFe ₃ O(O ₂ CPh) ₅ (pic) ₂ (EtOH) ₂ (H ₂ O)] ₂ (ClO ₄) ₂	-54.8, -41.8, -45.4, -63.2	10n

^a *J* values calculated with the $-2J\mathbf{S}_i\mathbf{S}_j$ Hamiltonian have been doubled for direct comparison with the ones determined here.

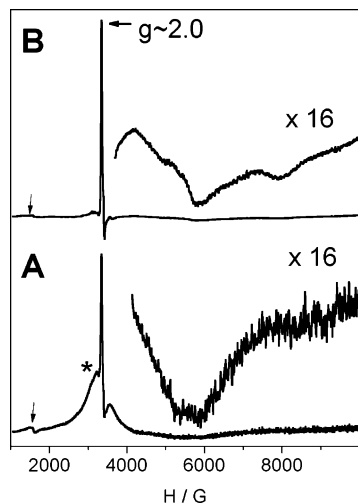


Figure 6. X-band (9.4 GHz) EPR spectra from powdered sample of **1a** (A) and from an acetone glass (B). The vertical arrows indicate the $g \sim 4.3$ signal attributed to ferric impurities. The asterisk in (A) indicates the broad signal at $g \sim 2.0$ which is absent in (B). EPR conditions: (A) temperature, 4.2 K; microwave power, 10 mW; modulation amplitude, 25 G_{pp}; (B) temperature, 5.1 K, microwave power, 2 mW, modulation amplitude, 25 G_{pp}.

X-Band EPR Spectroscopy. From the analysis of the magnetic susceptibility data, an isolated $S = 1/2$ ground state was deduced for **1a**. The analysis also indicated the presence of AE interaction. Further evidence for the presence of AE comes from X-band EPR studies (Figure 6). In the absence of AE the $S = 1/2$ state is expected to be characterized by the intrinsic \mathbf{g}_0 tensor of the transition metal ion. High-spin ferric ions are characterized by a fairly isotropic intrinsic \mathbf{g}_0 tensor. Therefore, the EPR signal from the $S = 1/2$ ground state should consist of a symmetric derivative feature at $g_{\text{eff}} \sim 2.0$. Indeed, such signals have been observed in the case of acetone solutions of [Fe₃(μ₃-O)(μ-O₂CPh)₅(salox)₁L₁L₂] (L₁ = L₂ = MeOH or L₁ = EtOH and L₂ = H₂O, H₂salox = salicylaldehyde).^{10h} However, the EPR spectra of several trinuclear ferric complexes, either in the solid state or in solution, deviate significantly from this case. In general, the spectra comprise one relatively sharp peak at $g_{\text{eff}} \sim 2.0$ and a broad tail at higher magnetic fields.²³ Such behavior is also

found for Cr₃ and Cu₃ complexes.^{24,25}

This characteristic EPR behavior has been successfully explained on the grounds of AE. Briefly, the AE term mixes the lowest two $S = 1/2$ states inducing an axial anisotropy in the \mathbf{g} tensor. The parallel component, g_{\parallel} , of the \mathbf{g} tensor lies along the direction of the antisymmetric pseudovector \mathbf{d} , assumed perpendicularly to the triangle plane. Because the g_{\parallel} component is not affected by the AE term, the EPR feature from this component consists of a rather sharp peak at a g value which coincides with the intrinsic \mathbf{g}_0 tensor. The axial component, however, strongly depends on this parameter. To a first approximation, for a high-spin triferric complex^{23a,26}

$$g_{\perp} = g_0 \left[\frac{\delta^2 - (hv)^2}{\Delta^2 - (hv)^2} \right]^{1/2} \quad (4)$$

where $\Delta = \sqrt{d^2 + 243d^2}$, hv is the energy of the microwave quantum (ca. 0.3 cm⁻¹ at X-band), and g_0 is the g value of the intrinsic \mathbf{g} tensor of the high-spin ferric ion (ca. 2.0). In this equation, δ is the separation of the two lowest $S = 1/2$ doublets in the absence of AE. For a strictly equilateral configuration (all three isotropic exchange parameters, J_{ij} 's, equal) $\delta = 0$. In this case the transition probability for an EPR signal at X-band vanishes.^{23a} For a lower symmetry (i.e., isosceles configuration) $\delta \neq 0$, and then EPR transitions are possible. Therefore, observation of an EPR signal from the $S = 1/2$ ground state constitutes evidence for nonequivalent exchange coupling constants, J_{ij} 's.

From eq 4, g_{\perp} is expected to be lower than g_0 and indeed signals corresponding to $g_{\text{eff}} \ll 2.0$ are observed in trinuclear complexes.²³ Inspection of eq 4 indicates that g_{\perp} is extremely sensitive in the parameters d and δ . This has the consequence that distributions in these parameters induce a large distribution in g_{\perp} . The broad high-field tails observed in these systems have been attributed to such distributions.^{23c,d,26}

In Figure 6A, we show the EPR spectrum of a powdered sample of **1a** recorded at liquid-helium temperatures. The spectrum exhibits a strong peak at $g \sim 2.0$ superimposed on a broad signal. Careful inspection of the spectrum reveals also the presence of broad features at higher magnetic fields. These signals are shown in a different scale. The broad spectrum on which the sharp peak is superimposed is attributed to intermolecular interactions present in the solid

(23) (a) Rakitin, Y. V.; Yablokov, Y. V.; Zelentsov, V. V. *J. Magn. Reson.* **1981**, *43*, 288–301. (b) Caneschi, A.; Cornia, A.; Fabretti, A. C.; Gatteschi, D.; Malavasi, M. *Inorg. Chem.* **1995**, *34*, 4660. (c) Sanakis, Y.; Boudalis, A. K.; Tuchagues, J.-P. *C. R. Chim.* **2007**, *10*, 116 and references therein.

(24) (a) Yablokov, Y. V.; Gaponenko, V. A.; Ablov, A. V.; Zhkhareva, T. N., *Sov. Phys. Solid State* **1973**, *15*, 251. (b) Nishimura, H.; Date, M. *J. Phys. Soc. Jpn.* **1985**, *54*, 395. (c) Honda, M.; Morita, M.; Date, M. *J. Phys. Soc. Jpn.* **1992**, *61*, 3773. (d) Vlachos, A.; Psycharis, V.; Raptopoulou, C. P.; Lalioti, N.; Sanakis, Y.; Diamantopoulos, G.; Fardis, M.; Karayanni, M.; Papavassiliou, G.; Terzis, A. *Inorg. Chim. Acta* **2004**, *357*, 3162. (e) Psycharis, V.; Raptopoulou, C. P.; Boudalis, A. K.; Sanakis, Y.; Fardis, M.; Diamantopoulos, G.; Papavassiliou, G. *Eur. J. Inorg. Chem.* **2006**, *18*, 3710.

(25) (a) Liu, X. M.; de Miranda, M. P.; McInnes, E. J. L.; Kilner, C. A.; Halcrow, M. A., *Dalton Trans.* **2004**, 59. (b) Yoon, J.; Mirica, L. M.; Stack, T. D. P.; Solomon, E. I., *J. Am. Chem. Soc.* **2004**, *126*, 12586. (c) Belinsky, M. I., *Inorg. Chem.* **2004**, *43*, 739. (d) Stamatatos, T. C.; Vlahopoulou, J. C.; Sanakis, Y.; Raptopoulou, C. P.; Psycharis, V.; Boudalis, A. K.; Perlepes, S. P. *Inorg. Chem. Commun.* **2006**, *9*, 814.

(26) Sanakis, Y.; Macedo, A. L.; Moura, I.; Moura, J. J.; Papaefthymiou, V.; Münck, E. *J. Am. Chem. Soc.* **2000**, *122*, 11855.

state. Such interactions have been considered in the analysis of the magnetic susceptibility data and have been observed in solid samples of other triferric complexes.^{10h,24e,27} In the present case, to minimize solid-state effects, we recorded a second EPR spectrum of **1a** dissolved in acetone (Figure 6B). The broad signal present in the solid sample is not observed in the acetone solution. Mononuclear high-spin ferric species usually give rise to characteristic signals at $g \sim 4.3$. The weakness of the $g \sim 4.3$ signal (which actually originates from impurities of the cavity) strongly suggests that no iron release in the form of high-spin ferric mononuclear takes place upon dissolution. On the other hand, the sharp $g \sim 2.0$ peak and the broad features at high magnetic fields are clearly retained in solution.

The EPR spectra of **1a**, either in the solid state or in solution, are attributed to the $S = 1/2$ ground state of the complex and are considered as evidence for the presence of AE interaction. Specifically, the sharp peak observed at $g \sim 2.0$ is attributed to the g_{\parallel} component. The broad features observed at higher fields are attributed to the g_{\perp} part of the axial signal. As discussed earlier, only a lower than equilateral symmetry would lead to an EPR active ground state. Therefore, observation of these signals is in line with the analysis of the magnetic susceptibility data, which was based on an isosceles rather than on an equilateral configuration. Application of the analytical eq 4 using the parameters of the exchange coupling constants and the magnitude of the antisymmetric parameter d derived from the magnetic susceptibility data yields a value of ca. 0.57 for g_{\perp} . The EPR spectra at the high magnetic field region, however, do not exhibit a feature corresponding to a well-defined g_{\perp} value. Instead, the broad high-field signals indicate a rather broad distribution with $g_{\perp} < 1.1-1.2$, which is in reasonable agreement with the value ($g_{\perp, \text{eff}} = 0.84$) derived from the magnetization data. As discussed above, the distribution in g_{\perp} are interpreted on the basis of distribution in J_{ij} 's and/or d . The slight line-shape differences observed in the high magnetic field signals in Figure 6A,B may result from differences in the distribution profiles between solid and solution phases.

Evidence for the presence of AE is provided on the basis of magnetic susceptibility measurements and X-band EPR spectroscopy. Moreover, EPR spectroscopy suggests also distributions in J_{ij} and/or the parameter d . Such distributions are probably not discernible in the magnetic susceptibility measurements, which under the above discussion reflect a mean over an unknown distribution.

Conclusion

Complexes of formula $[\text{Fe}_3(\mu_3\text{-O})(\mu\text{-LL})_6\text{L}_3]$ have been described for a variety of bridging LL ligands, including carboxylate, oxime, linked-pyridine/tetrazole, and now 4-nitropyrzazole, as well. With regard to the $\text{Fe}_3(\mu_3\text{-O})$ motif, both the Fe—O bond lengths and the Fe...Fe separations of **1** are

quite similar to those of the previously published structures (Table 3).¹⁰ Comparison of the spectroscopic (IR, Mössbauer) data (vide supra) also indicates that the $\text{Fe}_3(\mu_3\text{-O})$ motif is not significantly affected by the replacement of carboxylate by pyrazolate ligands, with the pyrazolate data resembling closer those of the benzoate.^{10b,e,h} In contrast, the magnetic data differ significantly between the pyrazolate and carboxylate materials (Table 6) with the former having a larger antiferromagnetic exchange value than the latter. The value of the antiferromagnetic exchange constant of **1a** falls close to those predicted by the models of Gorun and Lippard on the basis of the Fe—O distances, as well as by that of Christou et al. on the basis of Fe—O distances and Fe—O—Fe angles.^{11,28} Both models predict accurately J -values in polynuclear Fe^{III} systems that involve negligible contribution by a secondary magnetic exchange pathway. The J value predicted by the Gorun and Lippard relationship for **1** is approximately -70 cm^{-1} , while that of Christou et al. is -69.7 cm^{-1} , both $>5\%$ lower than the actual J value determined here (average J values of **1a** are -77.5 and -74.0 cm^{-1}). The latter are lower than the values calculated for and measured in $\text{Fe}_4(\mu_3\text{-O})_2$ “butterfly”-type complexes by Ruiz et al.²⁹ and the dioxime complex $[\text{Fe}_3\text{O}(\text{bamen})_3]^+$.^{10g} While the principal magnetic exchange path, Fe—O—Fe (a two-bond path), is practically identical in the pyrazolate and carboxylate complexes discussed here, the corresponding contributions of the secondary 3-bond (pyrazolate) versus the 4-bond (carboxylate) paths are evidently different. Pyrazolates have been known for a long time as efficient mediators of antiferromagnetic exchange,³⁰ and an important contribution of μ -pyrazolato ligands has recently been invoked for the interpretation of magnetic exchange among Cu^{II} centers.³¹ As a result, the overall antiferromagnetic exchange increases in magnitude in the case of the pyrazolate complex **1a** compared to its analogous carboxylates. This is also consistent with the higher degree of covalency of **1a** compared to its carboxylate analogues revealed by Mössbauer spectroscopy. Consequently, polynuclear pyrazolato complexes of open-shell metals are expected to show magnetic properties different from those of the corresponding carboxylates. Apart from the magnitude of the isotropic exchange interaction, the present complexes are also characterized by significant antisymmetric exchange.

Acknowledgment. Financial support of this work at the UPR was received from Grant NIH-SCoRE-5S06GM08102. D.P. acknowledges GAANN (Grant P200A030197-05) and RISE (Grant 2-R25-GM6-1151) doctoral scholarships. Financial support of the VEGA 1/2453/05 and APVT 20-005204 programs (R.B. and R.H.), of Slovakia, and Grant

(27) Boudalis, A. K.; Sanakis, Y.; Raptopoulou, C. P.; Terzis, A.; Tuchagues, J.-P.; Perlepes, S. P. *Polyhedron* **2005**, *24*, 1540.

(28) Cañada-Vilalta, C.; O'Brien, T. A.; Brechin, E. K.; Pink, M.; Davidson, E. R.; Christou, G. *Inorg. Chem.* **2004**, *43*, 5505.

(29) Cauchy, T.; Ruiz, E.; Alvarez, S. *J. Am. Chem. Soc.* **2006**, *128*, 15722.

(30) (a) Berends, H. P.; Stephan, D. W. *Inorg. Chem.* **1987**, *26*, 749. (b) Ehlert, M. K.; Rettig, S. J.; Storr, A.; Thompson, R. C.; Trotter, J. *Can. J. Chem.* **1989**, *76*, 1970.

(31) Koval, I. A.; van der Schilden, K.; Schuitema, A. M.; Gamez, P.; Belle, C.; Pierre, J.-L.; Lüken, M.; Krebs, B.; Roubeau, O.; Reedijk, J. *Inorg. Chem.* **2005**, *44*, 4372.

A Pyrazolate-Supported Fe₃(μ₃-O) Core

MSM6198959218 of the Ministry of Education, Youth and Sports of the Czech Republic (R.H.), is acknowledged.

Supporting Information Available: ORTEP diagrams (Figure S1) and X-ray data in CIF format (Figures S2–4) for **1a–c** and a

reconstruction of energy levels for **1a** (Figure S5). This material is available free of charge via the Internet at <http://pubs.acs.org>.

IC0701460